Astron. Astrophys. 362, 1158–1173 (2000)

ASTRONOMY AND ASTROPHYSICS

Modeling the number density distribution of interplanetary dust on the ecliptic plane within 5AU of the Sun

H. Ishimoto

Meteorological Research Institute, Japan Meteorological Agency, Nagamine 1-1, Tsukuba 305-0052, Japan (hishimot@mri-jma.go.jp)

Received 26 April 2000 / Accepted 31 August 2000

Abstract. We have used the relationship, consistent with observational data, between the radial dependence of the dust supply and the mass dependence of the number density distribution, to consider the parent bodies of interplanetary dust. We examine the number density distribution of the interplanetary dust within 5AU of the Sun on the ecliptic plane.

For the model calculations, the number density equations for the ecliptic plane are solved directly by taking into account collisional destruction between particles and the Poynting-Robertson effect, and by assuming a state of equilibrium and axial symmetry in the interplanetary dust cloud. Typical models for the radial dependence of the dust input on the ecliptic plane are considered. For three typical dust groups that are characterized by their orbits–i.e., bound particles, hyperbolic particles of collisional origin, and interstellar particles–a variety of simple models of the physical parameters are considered. These include the particles' optical properties, the mean sweep-out velocities of the dust clouds, the power law distribution of mass in the collisional fragments, the maximum size of particles, and the inner/outer boundaries.

From the model calculations, the existence of the three characteristic particle groups and their input radial dependencies are found to play important roles in determining the environmental conditions of interplanetary dust and the number density distribution of the particles. The roles played by comets and asteroids are estimated by analyzing the relationship between the radial dependence of the dust input and the resultant number density distribution at 1AU. To simulate the flux curve of interplanetary meteoroids at 1AU (e.g., Grün et al. 1985), a source that directly supplies the interplanetary dust is required. It is found that the simulated number density distribution fits that observed at 1AU well, if the mass production rate of dust sources outside 1AU increases with a radial index of $-3 \sim -4$ as the solar distance decreases. Such dust sources are more likely to be comets rather than asteroids.

The numerical results indicate that, at 1AU, cometary dust is the major component of particles with masses $m \geq 10^{-6}$g, and almost comparable in number to asteroidal particles with masses $10^{-12}\text{g} \leq m \leq 10^{-7}$g. Furthermore, we can expect that within 1AU the contribution of cometary particles increases as the solar distance decreases, due to the direct input of cometary particles.

In order for the results to be consistent with the observed $r^{-1\sim-1.3}$ radial dependence in the number density distribution of the zodiacal cloud inside 1AU, the mass production rate by the dust source should be almost constant or decreasing as the solar distance decreases.

Using a possible model for the dust sources and for the radial dependence of dust input, the number density of hyperbolic particles of collisional origin at 1AU is estimated to be $\sim 1.8 \times 10^{-4}\text{m}^{-2}\,\text{sec}^{-1}$.

Hyperbolic particles and the influx of interstellar particles ($m \sim 10^{-13}$g) inside 5AU increase the number density of interplanetary dust particles in the medium-sized range ($10^{-15}\text{g} \leq m \leq 10^{-6}$g). Interplanetary dust beyond 3AU of the Sun will, therefore, maintain a flat radial distribution of medium mass particles if the interstellar flux is significant.

Key words: inteplanetary medium – meteors, meteoroids

1. Introduction

It has been assumed that collisions between dust particles are an important process in maintaining the evolution of the zodiacal clouds. As already mentioned by Grün et al. (1985), for meteoroid flux at 1AU, the collisional timescale is shorter than the Poynting-Robertson orbital decay timescale for particles with masses $m \geq 10^{-5}$g. Since collisional fragmentation of large particles produces many small particles, the number density (or flux) distribution of interplanetary meteoroids may be changed significantly by the destruction of large particles. Furthermore, the small fragments which are generated may act to accelerate the collisional loss of large particles.

Within the same context, we can expect the size (or mass) distribution of interplanetary dust at 1AU also to be the result of the collisional evolution of particles under dusty environmental conditions, influenced by the dust production of their parent bodies and by the speed of the particles' orbital evolution. Although some attempts have been made to explain the flux distribution of interplanetary dust at 1AU (e.g., Mukai, 1989, Durda & Dermott, 1997), the results have not always been consistent with observations for the entire mass range. If we can reproduce the dust flux in the entire mass range by making some

assumptions about the conditions of the parent bodies, it may yield useful information on the origin of the interplanetary dust at 1AU.

Another important aspect is the number density of the interplanetary dust within 1AU of the Sun. Using the $r^{-1.3}$ dependence observed by Helios (e.g., Leinert et al., 1981), Leinert et al., (1983) concluded that this number density dependence is possible if there are sources inside 1AU that supply dust particles directly. On the other hand, analytical estimations based on observations by the IRAS and ZIP rockets in two wavelengths suggest that the number density of interplanetary dust shows a r^{-1} dependence (e.g., Levasseur-Regourd et al., 1991). Furthermore, this r^{-1} dependence is supported by ground-based observations of the solar F-corona (Mann & MacQueen, 1993). Since Leinert (1983) was not directly concerned with the radial change of particles' mass dependence in the number density distribution inside 1AU, the collisional evolution of interplanetary dust inside 1AU should be re-examined.

In this paper, the number density distribution of interplanetary dust is examined, taking into account particles' origins and collisional evolution. Furthermore, a quantitative model for the number density within 5AU is proposed that considers some of the aforementioned observational results. Finally, the resulting flux of hyperbolic particles and the effect of an influx of interstellar particles are also discussed.

2. Methods

2.1. Steady-state number density equations

The basic approach of this paper is the same as that in Ishimoto & Mann (1999) and in Ishimoto (1998). Some improvements to the calculations have been added for simplicity.

Assuming stable particle size distribution in time, and longitudinal homogeneity and latitudinal symmetry in the shape of the dust cloud, the number density distribution $n(m,r)$ of dust particles with the same latitudinal angle in a unit volume with mass m at a heliocentric distance r can be written (e.g., Ishimoto & Mann 1999):

$$\frac{\partial n(m,r)}{\partial r} = -\frac{n(m,r)}{r}\left(2+\frac{r}{|\overline{v_r}|}\frac{\partial|\overline{v_r}|}{\partial r}\right) + \frac{dt}{dr}\frac{dn'(m,r)}{dt}, \quad (1)$$

$$\frac{dn'(m,r)}{dt} = \frac{dn_{sup}(m,r)}{dt} + \frac{dn_{cg}(m,r)}{dt} - \frac{dn_{cl}(m,r)}{dt}, \quad (2)$$

where $\overline{v_r}$ is the mean radial velocity of the dust cloud at r in a state of equilibrium. $dn_{sup}(m,r)/dt$, $dn_{cg}(m,r)/dt$, and $dn_{cl}(m,r)/dt$ are, respectively, the dust supplied from parent bodies, the collisional gain, and the collisional loss. Transformation of the orbital inclination distribution in the dynamical and collisional process is neglected. Note that the same equations can be derived from Euler's equation of continuity.

2.2. Secular radial velocity of the dust

The value $\overline{v_r}$ in Eq. (1) is not equivalent to the radial velocity of particles in bound orbits, but rather to the sweeping velocity of a dust cloud at distance r. Orbital eccentricities and inclinations affect the radial velocity $\overline{v_r}$ of particles (and also dr/dt in Eq. (1)), the relative impact velocities between particles in $dn'(m,r)/dt$, and the probability of the existence of particles at r on the ecliptic plane. Since the probability of the existence of particles is reflected in the modeling of the radial dependence of dust input $dn_{sup}(m,r)/dt$, the value $\overline{v_r}$ in Eq. (1) includes the effect of eccentricity, but not the existence probability. According to Burns et al. (1979), the mean changes in the orbital perihelion distance q and the aphelion distance Q due to Poynting-Robertson drag are

$$\frac{dq}{dt} = -\frac{\beta GM_\odot(1-e)^3(4-e)}{2qc(1-e^2)^{3/2}} \quad (3)$$

$$\frac{dQ}{dt} = -\frac{\beta GM_\odot(1+e)^3(4+e)}{2Qc(1-e^2)^{3/2}}, \quad (4)$$

where c, G, and $M_\odot$ are the speed of light, the gravitational constant, and the mass of the Sun, respectively. β is the radiation pressure coefficient, which includes a factor due to solar wind. For a highly eccentric orbit, it is obvious that dr/dt at distance q is much smaller than that of a circular orbit, and dr/dt at distance Q is much larger. Another aspect to consider is that $\overline{v_r}$ in Eq. (1) is the value for an equilibrium state. This means that we have to consider the existence of particles with less eccentric orbits due to dynamical evolution by Poynting-Robertson drag. For example, when the original orbit described in Eqs. (3)-(4) is changed by Poynting-Robertson drag, and the orbital aphelion distance Q' becomes q, dQ'/dt is

$$\frac{dQ'}{dt} = -\frac{\beta GM_\odot(1+e')^3(4+e')}{2Q'c(1-e'^2)^{3/2}}, \quad (5)$$

where e' is obtained from the integration of Eqs. (3)-(4) (e.g. Wyatt & Whipple, 1950),

$$\text{const.} = q(1+e)e^{-4/5} = Q'(1-e')e'^{-4/5}, \quad q = Q'. \quad (6)$$

Conclusively, for one input orbit, there are particles with various orbital eccentricities in the range e' to e at distance r ($r = q = Q'$) in the equilibrium state. If we take an original eccentricity of $e = 0.9$, e' becomes about 0.27, and the radial velocity lies in the range $0.0094v_c$ to $2.4v_c$, where v_c is the radial velocity of a circular orbit. Therefore, for a solar distance r ($r \le q$), v_c is always within the range of the radial velocity, even for highly eccentric orbits.

In this work, we adopt the mean radial velocity $\overline{v_r}$ for bound orbits as

$$\overline{v_r} = \frac{dr}{dt} \sim v_c = -\frac{2\beta GM_\odot}{rc}, \quad \beta = \beta_{PR}(1+\delta) \quad (7)$$

where β_{PR} is the ratio of solar radiation pressure to solar gravity, and $\delta(\sim 0.35)$ is a factor owing to the solar wind (Burns et al., 1979). The typical interplanetary dust material is assumed

to be "astronomical silicate" (Draine & Lee, 1984); its optical constants are adopted for β_{PR} with particle mass m. Although Eq. (7) appears to assume only circular orbits, this treatment can be used as a first order approximation, even for a dust population with orbits that were originally highly eccentric, at least inside their average perihelion distance. For original dust orbits outside the average perihelion distance, Eq. (7) can be assumed to be the lower estimation.

2.3. Transition between bound and hyperbolic orbits

This paper considers three particle groups, characterized by their orbits: the main particles in bound orbits, interstellar particles, and particles in hyperbolic orbits. The perihelion distance of a particle in hyperbolic orbit is considered to be the same as the solar distance of the point of generation. When particles originate from their parent bodies (or from target particles in collisions), they are assumed to be in hyperbolic orbits if their β values exceed a critical value β_c,

$$\beta_c = \beta_0 + \frac{(1-e^2)(1-\beta_0)}{2(1+e\cos\phi)} \tag{8}$$

where β_0 is the value for target particles, and ϕ is the true anomaly of the parent orbit. As shown in Eq. (8), β_c depends on the release point ϕ as well as on the eccentricity of the parent orbit. For particles originally released from comets, for example, the release points are near the perihelion of the comet orbits, and a lot of ejecta particles take hyperbolic orbits because of the high eccentricity of the parent comets. In the numerical calculations in this paper, we implicitly omit these hyperbolic particles originally released from parent bodies; rather, we discuss those generated by collisions between particles. Such hyperbolic particles can be produced elsewhere in the eccentric orbit of the parent particles, and β_c has a range

$$\frac{1+\beta_0-e(1-\beta_0)}{2} \le \beta_c \le \frac{1+\beta_0+e(1-\beta_0)}{2} \tag{9}$$

For a first order approximation, the averaged value of β_c is applied,

$$\beta_c \sim \frac{\beta_0+1}{2}. \tag{10}$$

Since β_c is used only for an average boundary that distinguishes the population of hyperbolic particles from particles with bound orbits, this simplification will not lead to any critical defects in the results of the numerical calculations, except in the smoothness of the resultant curves of the number density distribution.

2.4. Collisions between grains

Three types of collisions are then combined to obtain $dn_{cg}(m,r)/dt$ and $dn_{cl}(m,r)/dt$.

$$\frac{dn_{cg}(m,r)}{dt} = \frac{dn_{mg}(m,r)}{dt} + \frac{dn_{ig}(m,r)}{dt} + \frac{dn_{hg}(m,r)}{dt}, \tag{11}$$

$$\frac{dn_{cl}(m,r)}{dt} = \frac{dn_{ml}(m,r)}{dt} + \frac{dn_{il}(m,r)}{dt} + \frac{dn_{hl}(m,r)}{dt}. \tag{12}$$

The subscripts on the right side of Eqs. (11) and (12) denote the type of projectile, where the mg, ig, and hg terms represent the gains of particles with mass m due to collisions with, respectively, the main particles, the interstellar particles, and the hyperbolic particles (the ml, il, hl terms are the same, but for collisional losses).

The collisional gain and loss terms are calculated by using the following equations (e.g., Grün et al., 1985)

$$\frac{dn_g(m,r)}{dt} = \int\int g(m_p,m_t,m)\, n(m_t,r) \cdot n(m_p,r)\, v_i(r)\, \sigma(m_p,m_t)\, dm_p\, dm_t, \tag{13}$$

$$\frac{dn_l(m,r)}{dt} = n(m,r) \int n(m_p,r)\, v_i(r) \cdot \sigma(m,m_p)\, dm_p, \tag{14}$$

where m_p and m_t are the masses of the projectile and the target respectively, and σ is the collisional cross section. The mean impact velocity $v_i(r)$ for collisions between the main particles, $0.53 \times v_k$, is applied, assuming $\sim 16\,\mathrm{km\,s^{-1}}$ at 1AU. Although this mean impact velocity on the ecliptic plane at 1AU is derived from preliminary calculations, which take into account dispersion in orbital inclination ($\sigma_i = 30^o$) and orbital evolution due to Poynting-Robertson drag with initial orbital eccentricity $e = \beta/(1-\beta)$, it is an acceptable value when compared with observations (e.g. McDonnell, 1978) for particles in the middle mass range on bound orbits. For collisions between the main and interstellar particles, we adopt $\sqrt{v_k^2+v_s^2}$, where v_k is the Keplerian velocity at distance r, and $v_s (\sim 26\,\mathrm{km\,s^{-1}})$ is the influx velocity of interstellar particles observed by Ulysses (Grün et al., 1993). For impacts by hyperbolic particles, $v_i(r)$ is estimated numerically throughout these calculations.

In the numerical calculations, erosive collisions are also taken into account, as well as catastrophic destructions. The value $g(m_p,m_t,m)$ in Eq. (13) is the production of particles with mass m due to collisions between a projectile and a target, and a simple power law distribution has been adopted, namely,

$$g(m_p,m_t,m) = (\gamma-1)m_x^{\gamma-1}m^{-\gamma} \quad (m_x \ge m)$$
$$= 0 \quad (m_x < m) \tag{15}$$

$$m_x = \frac{2-\gamma}{\gamma-1}\, B\cdot E \quad (m_t > B\cdot E)$$
$$= \frac{2-\gamma}{\gamma-1}\, m_t \quad (m_t \le B\cdot E), \tag{16}$$

where m_x denotes the mass of the largest fragment, and E is the impact energy of the collision ($B\cdot E$ is the cratering mass). Assuming the material is chondritic rock (i.e., Banaszkiewicz & Ip, 1991), a value of 4×10^{-9}(in cgs units) has been adopted for B. Symbol γ stands for the mass index. Since the fragmentation process for impacts between small particles is not precisely known, a value of $\gamma = 5/3$, analogous to the results of laboratory experiments (Nakamura & Fujiwara, 1991), has been

adopted. To calculate the impact energy E, the effect of oblique impacts has been taken into account (Tielens et al., 1994). Impact vaporization has been neglected for simplicity.

2.5. Calculation of the number density of hyperbolic particles

The number density distribution of hyperbolic particles is obtained by substituting the following equations into Eq. (1), under the assumption that the point of generation of a hyperbolic particle becomes its orbital perihelion (see Ishimoto & Mann, 1999).

$$\frac{r}{|\overline{v_r}|}\frac{\partial|\overline{v_r}|}{\partial r} = \left(\int_{r_0}^{r}\frac{\frac{dn_h(r',m)}{dt}r'\left[r'-r(1-\beta)\right]}{r^2(2\beta-1)+2rr'(1-\beta)-r'^2}dr'\right) \Big/ \left(\int_{r_0}^{r}\frac{dn_h(r',m)}{dt}dr'\right), \quad (17)$$

$$\frac{dt}{dr} = \frac{1}{\Delta r}\sqrt{\frac{-a^3}{GM_\odot(1-\beta)}}\left(e\sinh u - u\right), \quad (18)$$

where $n_h(r',m)$ is the number density distribution for the hyperbolic particles, and

$$a=\frac{r-\Delta r}{1-e},\quad \cosh u=\frac{1}{e}\left(1-\frac{r}{a}\right),\quad e=\frac{\beta}{1-\beta}.$$

Δr is the radial step in the calculations. Since the numerical estimations for the number density are performed by $n(r+\Delta r)=n(r)+\Delta r\partial n(r)/\partial r$, the dependence of Δr in Eq. (18) vanishes in the actual calculations.

2.6. Maximum size of particles

As defined in Eq. (7), the mean orbits of the main particles are assumed to be changed by Poynting-Robertson and solar wind drag forces. As the particles become larger, the timescale of the radial drift lengthens; Eq. (7) will be inadequate for very large particles, because other dynamic effects (i.e., planetary perturbations) may change their mean orbits faster than the P-R and solar wind drag forces. Since the radial velocity denoted here is the mean sweep-out velocity of the dust clouds, we cannot derive a maximum size simply by comparing the strengths of the Poynting-Robertson drag and the planetary perturbation effects. Even if planetary perturbations affect particle orbits more than Poynting-Robertson drag, the latter can still be the dominant force for the radial velocity considered if planetary perturbations do not sweep out the dust clouds in that region. As a test case, the maximum ejecta mass of the two sources is set to 1kg. Although there is no particular reason for this choice, the value is consistent with that estimated from cometary activities (e.g. Keller, 1990).

2.7. Inner and outer boundaries

The inner boundary of zodiacal dust clouds will be around the edge of a dust free zone, within which particles are vaporized by solar heating. Although such vaporization would depend on the size and chemical composition of particles as well as on their shape (e.g. Kimura et al., 1998), an inner boundary r_0 of 0.02AU (~ 4 solar radii) is used in these calculations for simplicity.

For the outer boundary, a distance of 5AU from the Sun has been assumed because of Jovian gravitational perturbations. Because these perturbations will have a critical effect on the dust environment around 5AU–not only on particles' orbits but also on dust supply from parent bodies–it is not appropriate to set the outer boundary at beyond 5AU in these model calculations. Nevertheless, it is easy to take into account the influence of dust particles coming from far beyond Jupiter's orbit (i.e. EKO dust), if we know how much dust can pass through. Although some dust particles generated far beyond 5AU may contribute to the zodiacal dust cloud within 5AU (e.g. Flynn, 1994, Liou et al., 1996), the influence of such particles is neglected because of the lack of information on their fluxes.

2.8. A sketch of the algorithm for solving the number density equations

Since the collisional process is fundamentally not time-reversible, for the main particles, the calculation of Eq. (1) has to start from the outer boundary and continue sunward. On the other hand, for hyperbolic particles, the calculation of Eq. (1) has to start from the inner boundary and continue outward by using Eq. (18). Therefore, the numerical calculations are performed in the following way: (i) Eq. (1) is calculated from the outer boundary sunward, with no influence from generated hyperbolic particles, and the production of hyperbolic particles at an arbitrary solar distance r is estimated. (ii) From the results of (i), Eq. (1) is calculated for the generated hyperbolic particles, from the inner boundary outwards, without any influence from the main and interstellar particles, and the flux of hyperbolic particles at distance r is derived. (iii) Procedure (i) is performed again, taking into account the collisions between the hyperbolic and main particles, using the results from (ii). The iterative calculations of (ii) and (iii) are continued until the number density distributions of the main and hyperbolic particles becomes stable. For the numerical calculations, a radial step $\Delta r = 10^{-4}$AU is used.

3. Modeling dust production outside 1AU

3.1. Preliminary calculations

Since the dust production rate and its radial dependence at an arbitrary solar distance are not known exactly, preliminary calculations are necessary. For simplicity, two dust sources are assumed, where one (A) has a constant dust production rate between 2AU and 3AU, and the other (C) has a broader radial distribution with a radial dependence $dn_{sup}/dt \propto r^{-\alpha}$ for $r \geq 1$AU (see Fig. 1). Although these two models of dust production indicate dust production by asteroids and by comets, in order to generalize the relationship between the resultant number density distribution and the radial dependence of the dust input we shall not discuss the radial distribution of asteroidal and cometary dust directly and in detail here. Rather we employ

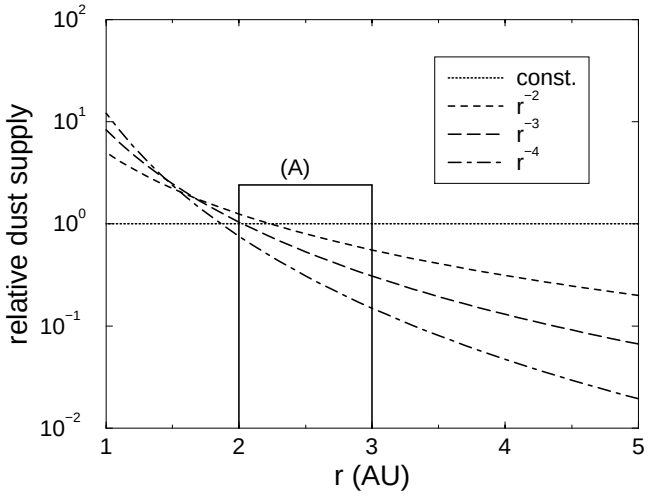

Fig. 1. The assumed relative values of the dust production rate by source (A) (solid line) and source (C). For source (C) particles, a few different radial dependencies for dust production are assumed. The total dust production between 1AU and 5AU for the source (C) cases is the same as that in the constant case (dotted line).

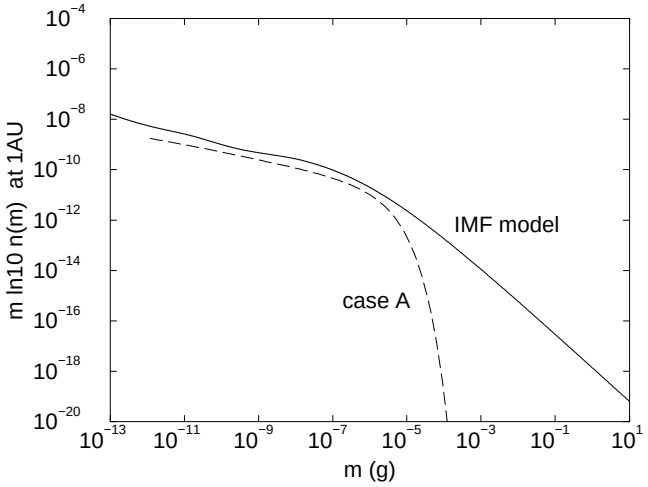

Fig. 2. The calculated number density distribution at 1AU for particles from source (A) (long-dashed line). The dust input between 2AU and 3AU is 1.1×10^{-33}kg m^{-3} sec^{-1} (see, Fig. 1). The solid line corresponds to the IMF model at 1AU.

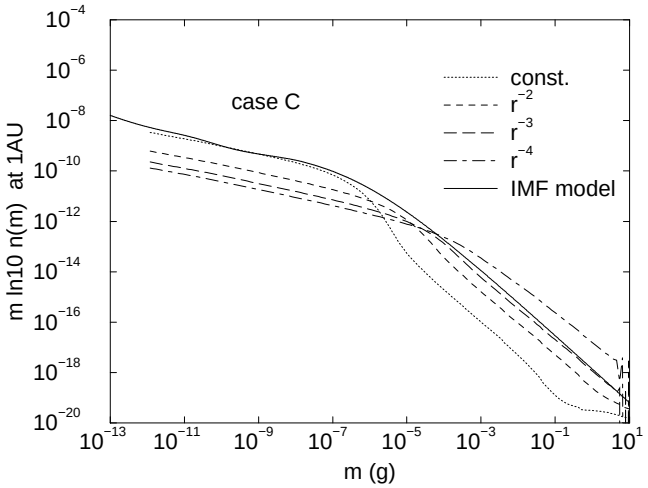

Fig. 3. Same as Fig. 2 but for source (C) particles. A dust production rate of 4.5×10^{-34}kg m^{-3} sec^{-1} is adopted in the constant case (dotted line). The solid line corresponds to the IMF model at 1AU. The other lines denote the results for the other radial dependencies shown in Fig. 1.

a more simple form for the radial dependence of the dust input than that used in our previous work (e.g. Ishimoto, 1998). We examine the value α by comparing the resultant number density distribution with that of observational data at 1AU, without assuming anything about comets or cometary particles. The radial dependence of the dust production rate on the ecliptic plane depends on the existence probability of particles in their orbits, and therefore potentially includes the effects of orbital eccentricity as well as the inclination of the parent bodies. In our approach, we take the radial dependence of the dust input on the ecliptic plane as an unknown parameter, but this does not mean that we neglect the particles' orbital eccentricities and inclinations in our model calculations. The relationship between the orbital elements and the radial dependence of the dust input is briefly discussed in Sect. 3.4.

For the preliminary calculations performed in this section, the existence of hyperbolic and interstellar particles is not considered, and only collisions between the main particles and the dust supplied by their sources is taken into account. Therefore only procedure (i) of the previous section is required. Since interstellar and hyperbolic particles are neglected, the number density distribution is calculated for particles with masses $m \geq 10^{-12}$g.

In order to evaluate the radial dependence of dust sources, we compared the calculated particle mass distribution at 1AU with the Interplanetary Meteoroids Flux (IMF) model (Grün et al., 1985). Note that recent observational results by LDEF are consistent with the flux distribution deduced by the IMF model at 1AU, for particles larger than $10\,\mu$m (e.g. McDonnell et al., 1996).

Fig. 2 shows the resulting mass distribution at 1AU for case (A). In order for the resultant number density distribution for masses $10^{-12}\text{g} < m < 10^{-6}$g to be comparable with that of the IMF model at 1AU, the dust production rate was set to 1.1×10^{-33}kg m^{-3} sec^{-1}. Particles with masses $m \leq 10^{-6}$g significantly contribute to the flux at 1AU. On the other hand, there is a large gap between our numerical result and the IMF model for particles with masses $m \geq 10^{-5}$g. Since collisional loss affects large particles, and since there is no dust input within 2AU of their parent bodies, a steep decrease in the number density distribution occurs in case (A).

The results for case (C) are shown in Fig. 3. The dust production rate on the ecliptic plane was selected as 4.5×10^{-34}kg m^{-3} sec^{-1} in the case where dust input is constant ($\alpha = 0$). The other lines in Fig. 3 correspond to dust production rates with different radial dependencies, calculated under the assumption that the total dust input on the ecliptic plane

between 1AU and 5AU is the same as that in the constant case (see Fig. 1).

3.2. Typical mass dependence in collisional evolution

If the dust input locations include the observing point (1AU), the observed number density distribution for particles with masses $m \geq 10^{-12}$g tends to have a typical mass dependence. An explanation has been proposed by Ishimoto (2000). For simplicity, the mass distribution of the dust supply $dn_{sup}(m,r)/dt$ is supposed to be described by the same power law with index γ as that of collisional fragmentation ($dn_{sup}(m,r)/dt = C_0 m^{-\gamma}$). The collisional gain dn_g/dt is given approximately by Eq. (13)

$$\frac{dn_g(m,r)}{dt} \sim C_1 m^{-\gamma}. \tag{19}$$

Assuming that the number density distribution can be written as $n(m,r) = p(m)t(r)$, and that the collision target of mass m is considerably larger than the projectile, Eq. (14) becomes approximately,

$$\frac{dn_l(m,r)}{dt} \sim C_2 p(m) m^{\frac{2}{3}}. \tag{20}$$

The coefficients C_0, C_1, C_2 in the above equations have no dependence on particle mass m. Using Eqs. (1)-(7) and $\beta \propto m^{-1/3}$, $p(m)$ can be written as

$$p(m) \propto m^{\frac{1}{3}} \left[(C_0 + C_1) m^{-\gamma} - C_2 p(m) m^{\frac{2}{3}} \right]. \tag{21}$$

If the value of the total number density is small, and the collisional gain and loss are negligible ($C_1, C_2 \to 0$), then

$$p(m) \propto m^{-\gamma+\frac{1}{3}}. \tag{22}$$

As the total number density increases, collisions between particles become effective. In such a situation, the number density distribution will show two typical mass dependencies. For small particles, the loss term is considerably smaller than the gain term. Therefore, the mass dependency of $p(m)$ becomes

$$p(m) \propto m^{-\gamma+\frac{1}{3}}. \tag{23}$$

On the other hand, collisional loss affects large particles, and the loss term balances the gain term in a steady state. Therefore,

$$p(m) \propto m^{-\gamma-\frac{2}{3}}. \tag{24}$$

As a result, in a region where dust is produced from the parent bodies, the number density distribution of the dust cloud will tend to form two slopes with $m^{-\gamma+1/3}$ and $m^{-\gamma-2/3}$ dependencies in mass. For large particles, the dust cloud will maintain this collisional balance if dust production from the parent bodies increases (or remains constant) as the solar distance decreases. However, once the dust cloud passes the region of peak dust input, the collisional balance for large particles is broken. The mass dependency for large particles then shows a sudden drop, as shown in case (A) (see Fig. 2). This loss of collisional balance occurs not only in the case where dust input stops at an arbitrary solar distance r, but also when dust production decreases as the heliocentric distance decreases. Although some of the asteroidal particles may be supplied directly at 1AU, the general trend of the number density distribution for the entire population at 1AU will be the same as that in Fig. 2, because most asteroidal particles are initially supplied from a region far from the inner edge of the asteroid belt ($\sim$ 2AU).

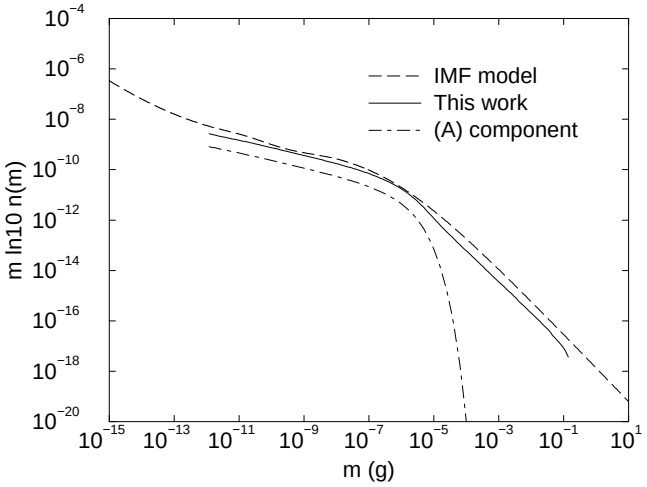

Fig. 4. The calculated number density distribution at 1AU for the combined dust sources (solid line). The values $1.4 \times 10^{-32} r^{-3.5}$kg m^{-3} sec^{-1} and 1.1×10^{-33}kg m^{-3} sec^{-1} are adopted for the dust production rates in sources (C) and (A) respectively. The result for the (A) component is shown by the dash-and-dotted line.

Assuming continuous dust production and using simple algebra, $p(m)$ can be expressed by using a reference value $p(m_c)$ as

$$p(m) = \frac{2\left(\frac{m}{m_c}\right)^{-\gamma+\frac{1}{3}}}{1+\left(\frac{m}{m_c}\right)} p(m_c), \tag{25}$$

where m_c is the critical mass of the particles. The slope of the distribution $p(m)$ changes around m_c, meaning that the physical process described by Eq. (23) changes to that described by Eq. (24) around this point. If we assume a typical value of $-5/3$ for the mass index $-\gamma$ for the dust supply, and $m_c \sim 10^{-6}$g, the resultant mass dependence of the number density distribution shows good agreement with that predicted by the IMF model for particles with masses $m \geq 10^{-12}$g. We can expect that, at 1AU, collisional balance affects particles with masses $m \geq 10^{-5}$g. This indicates that, at 1AU, the dust source supplies particles with mass $m \geq 10^{-5}$g directly, with a radial dependence of $r^{-\alpha}$ ($\alpha \geq 0$).

3.3. Radial dependence of dust input outside 1AU

From Figs. 2 and 3, the absolute values and mass dependence of the number density distribution for particles with masses $m \geq 10^{-5}$g depend on the radial index α of the dust source, while those for particles with $10^{-12}\text{g} \geq m \geq 10^{-6}$g depend mainly on the total dust production beyond 1AU. Furthermore, from

Fig. 3, one finds that the dust source that gives the $m \geq 10^{-5}$g number density distribution at 1AU has a radial index $3 < \alpha < 4$ between 1AU and 5AU.

Fig. 4 shows the numerical result at 1AU, taking into account the (A) and (C) dust sources outside 1AU. Values of $1.4 \times 10^{-32} r^{-3.5}$kg m^{-3} sec^{-1} (where r is in AU), and 1.1×10^{-33}kg m^{-3} sec^{-1} have been adopted for the dust inputs of the (C) and (A) components respectively. It should be noted that, at 1AU, the number density distribution of the (A) component at masses $10^{-12}\text{g} \leq m \leq 10^{-6}$g can be changed easily if the dust production rate is changed, and our numerical result does not change drastically, even if we assume that most of the particles at 1AU with $10^{-12}\text{g} \leq m \leq 10^{-6}$g have the same origin as that of component (A). However, in order to simulate the same flux curve for particles with $m > 10^{-6}$g as that of the IMF model, a significant (C) component, with the mass production rate and radial dependence described above, is necessary.

The validity of the mass production rate adopted for source (A) for asteroidal particles has not been checked because of some difficulties. Since the recent orbits of asteroids are the result of planetary perturbations over a long time scale, they may not be derived exactly if we apply simple estimations such as the "particle-in-a-box" approximation, based on the observed orbital elements of asteroids. Furthermore, the number and size distribution of small asteroids are still ambiguous. However, it is acceptable to assume an important contribution by asteroidal dust in the zodiacal cloud. In order to simulate the IMF number density distribution at 1AU over the entire mass range, the mass production rate for the source (A) is not very important, as long as the mass produced is not too great to explain the IMF values of $10^{-12}\text{g} \leq m \leq 10^{-6}$g. Rather, the problem is whether comets can sustain the mass production rate for source (C) with the radial dependence noted above. As shown in Fig. 4, source (C) particles can sustain $10^{-12}\text{g} \leq m \leq 10^{-6}$g particles at the same order of magnitude as the IMF at 1AU, even if we neglect the existence of source (A) particles.

3.4. Rough estimations of cometary dust production for source (C) particles

Here, an order of magnitude estimation for the mass produced by comets is calculated. The average mass produced $\overline{M}_j$ (kg sec^{-1}) can be estimated approximately as

$$\overline{M}_j \sim \frac{2}{T_j} \int A_j dt, \tag{26}$$

where T_j is the orbital period of the comet and $A_j(r)$ is the comet's activity. If we assume that the activity A_j has a radial dependence $r^{-\varepsilon}$,

$$A_j \sim \frac{\pi R_j^2 L_\odot (1 - A_b)\chi}{L_h} \left(\frac{r}{r_\oplus} \right)^{-\varepsilon} \tag{27}$$

where R_j, A_b, $L_\odot$, L_h, and χ are, respectively, the radius and surface albedo of the comet, the solar luminosity at Earth orbit, the cometary material's latent heat, and its dust to total mass ratio. $r_\oplus$ is the orbital radius of the Earth. Using an orbital semi-major axis a_j, a perihelion distance q_j, and an aphelion distance Q_j for the comet,

$$\frac{dr}{dt} = G^{\frac{1}{2}} M_\odot^{\frac{1}{2}} a_j^{-\frac{1}{2}} \left(1 - \frac{q_j}{r}\right)^{\frac{1}{2}} \left(\frac{Q_j}{r} - 1\right)^{\frac{1}{2}}, \tag{28}$$

$\overline{M}_j$ can be estimated approximately as

$$\overline{M}_j \sim \frac{R_j^2 L_\odot (1 - A_b)\chi}{a_j L_h} \int_{q_j}^{r_c} \left(\frac{r}{r_\oplus} \right)^{-\varepsilon} \cdot \left(1 - \frac{q_j}{r}\right)^{-\frac{1}{2}} \left(\frac{Q_j}{r} - 1\right)^{-\frac{1}{2}} dr. \tag{29}$$

where r_c is the critical distance outside which the comet becomes inactive. Then, the mass production rate $dM(r, \lambda)/dt$ at a solar distance r on the ecliptic plane (latitude: $\lambda = 0$) is

$$\frac{dM(r, 0)}{dt} = \sum_j \overline{M}_j n(r, 0), \tag{30}$$

where $n(r, 0)$ is the spatial density when the dust plume is distributed in an axially symmetric shape, which is given by (e.g. Kessler, 1981)

$$n(r, 0) = \frac{(1 - \bar{e})^{\frac{3}{2}}}{2\pi^3 r \bar{q} (r - \bar{q})^{1/2} \left[\bar{q}(1 + \bar{e}) - r(1 - \bar{e})\right]^{1/2} |\sin \bar{i}|}. \tag{31}$$

$\bar{q}$, $\bar{e}$, $\bar{i}$ are the mean orbital elements of the ejecta. For long period comets, ejected particles can easily escape from the solar system because of the comets' eccentric orbits and the additional forces exerted by solar radiation, and hence the value of $n(r, 0)$ is small. On the other hand, particles ejected by short period comets can survive in the solar system relatively easily. According to the observed mass distribution of particles ejected from comet P/Halley (Mazets et al., 1986), the total mass of the ejecta depends on the particles with large masses. Furthermore, such large ejecta will have orbits similar to those of the parent comet ($\bar{q}, \bar{e}, \bar{i} \sim q_j, e_j, i_j$). Under these assumptions, numerical calculations of Eq. (30) for known short period comets have been performed. For A_b, χ and L_h, typical values for cometary material are used. These are $A_b = 0.05$, $\chi = 2/3$ and $L_h = 5.1 \times 10^7$J kg^{-1} (Lamy, 1974). Moreover, for simplicity a typical size of $R_j = 1$km for all short period comets is adopted. The results are shown in Fig. 5. Although differences appear between the results for model (C) and those for short period comets, model (C) is not unrealistic in the region beyond 1AU, given the rough estimations of the physical properties of short period comets adopted here.

Another point to note is the mean radial velocity $\overline{v_r}$ for cometary dust clouds. As denoted in Sect. 2, for $r > 1AU$ the $\overline{v_r}$ applied in our calculations for model (C) may be much lower than that of actual cometary clouds, because of comets' high eccentricities and their perihelion distances ($\sim$ 1AU). As the radial velocity becomes faster, collisional evolution becomes slower. Therefore, collisional erosion for large cometary particles may be less active than model (C) suggests. It is possible that the

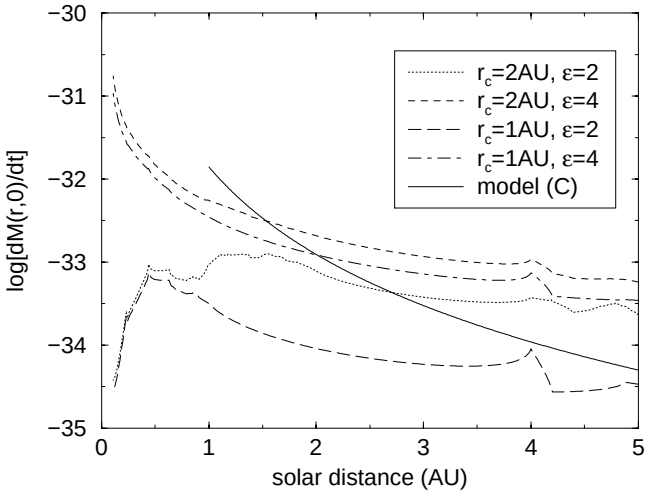

Fig. 5. The estimated rate of dust production by known short period comets on the ecliptic plane for different values of r_c and ε (see, Eq. (29)). The derived values have been averaged within ± 0.1AU. The solid line denotes the modeled dust production by source (C).

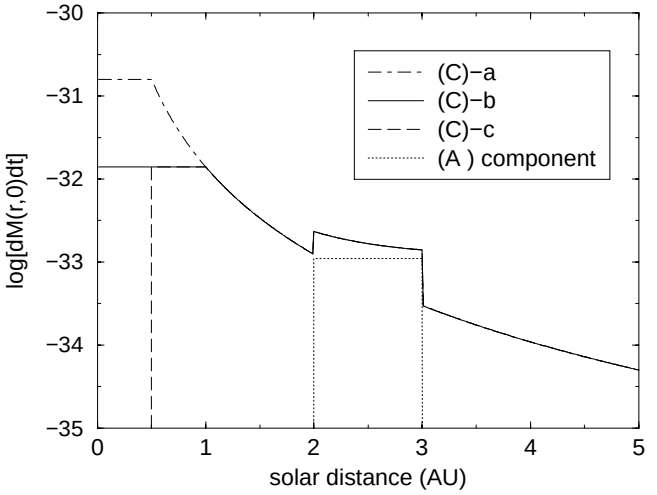

Fig. 6. The rate of mass production by the assumed dust sources on the ecliptic plane, as a function of heliocentric distance. Three scenarios for radial dependence inside 1AU ((C)-a, (C)-b, and (C)-c) are considered. See text for details.

higher radial velocity of cometary particles outside 1AU can sustain a number density distribution of $m > 10^{-6}$g particles at 1AU even for a flat radial dependence in the mass input.

In Fig. 4, most of the particles that originate from source (C) with masses $10^{-12}\text{g} \leq m \leq 10^{-6}\text{g}$ are not the original ejecta from source (C), but are fragments of large source (C) particles, caused by collisions after ejection. If only the original ejecta from comets are considered, it is difficult to sustain the total flux of interplanetary dust in the typical size range (about several tens of microns) contributed by known short period comets. However, if the collisional fragmentation of large cometary particles is taken into account, it is not difficult to maintain the total dust flux at 1AU solely by the contributions of known short period comets. Since the total mass of the ejecta depends on the particles with large masses, we do not need to be too concerned about small particles that have their initial orbits changed drastically by solar radiation pressure after being ejected from the comets. It is therefore expected that the cometary dust trails formed by large cometary particles (e.g. Sykes & Walker, 1992) are important secondary sources of cometary dust.

4. Modeling dust production inside 1AU

The numerical models of dust sources and the resultant number density distribution described in the previous section are preliminary and not final. Nevertheless, the basic appearance of the number density distribution at 1AU for particles with masses $m \geq 10^{-12}$g, and the points discussed in the previous section are the same, even when interactions of interstellar and hyperbolic particles are taken into account. In order to consider interactions between the main and the hyperbolic particles, it is necessary to estimate the production rate of the latter. Therefore, modeling of the interplanetary dust cloud inside 1AU is required to model the dust environment inside as well as outside 1AU.

As shown in Fig. 5, the mass production rate within 1AU depends strongly on the mean activities of short-period comets. In particular, the role of several short period comets that reach relatively close to the Sun, i.e., P/Encke, is important (e.g. Liou et al., 1995) because of their large contribution to the total mass input within 1AU. Furthermore, this indicates a considerably large time fluctuation in the dust production rate inside 1AU due to the orbital evolution of the comets and the lifetime of the comets' activities. Therefore, estimation of the mean dust production rate within 1AU implicitly contains considerable ambiguity. For the models presented in this paper, the roles played by specific comets in dust production and their contribution to ejecta particles in the zodiacal cloud are not discussed. Instead, rough estimates of the mass production rate within 1AU are obtained, and the resultant particle number density distributions are discussed by comparing them with observational results inside 1AU. In particular, the radial dependence of the number density of medium-sized particles, observable as zodiacal light, is a good indicator for checking the derived results. From analysis of ground-based observations and in-situ spacecraft measurements (mainly by Helios), the number density of interplanetary dust is considered to have a radial dependence of $r^{-1\sim1.3}$ on the ecliptic plane (e.g. Leinert et al., 1981, Levasseur-Regourd et al., 1991).

Here, three types of radial dependence are examined for the mass production rate of dust sources (C) within 1AU (see Fig. 6). There are no strong physical motivations for their selection; they only determine whether the mean mass production rate within 1AU increases or decreases as the heliocentric distance decreases. The numerical calculations are performed for particles with masses $m \geq 10^{-15}$g, taking the existence of hyperbolic particles into account, and include the iterations described in Sect. 2. In these calculations, the existence of interstellar flux is not considered.

4.1. Results of model calculations

Fig. 7 shows the calculated number density distribution at 1.0AU, 0.5AU, and 0.1AU for the three cases of dust input described in Fig. 6. For spherical particles of "astronomical silicate" in our model calculations, particles with 10^{-15}g $\leq m \leq 10^{-12}$g generated by collisions with large particles become hyperbolic. Most of the hyperbolic particles in the calculations are then within this mass range. Note that, because of our simple division between bound and hyperbolic particles in Eq. (10), some particles in bound orbits will also exist in this mass range, as well as hyperbolic particles with $m > 10^{-12}$g and $m < 10^{-15}$g.

The number density distribution of hyperbolic particles at an arbitrary solar distance r depends on their production rate inside r, whereas that of the main particles depends on the production rate outside r. Therefore, there is no physical requirement for the flux of the two dust populations to be comparable at distance r. From the 1AU plots in Fig. 7, the number density for masses 10^{-14}g $\sim 10^{-12}$g is about two orders of magnitude smaller than that of the IMF model. Since, for the IMF model, the transformation from cumulative flux to number density distribution assumes a constant impact velocity of 20 km sec^{-1} (see Grün et al., 1985), and our calculated impact velocities for the hyperbolic particles at 1AU are much higher than 20 km sec^{-1}, the difference in absolute number density between our numerical results and those of the IMF model can be reduced if the same treatment is adopted for our model (see the long-dashed lines in Fig. 7). However, even if such a transformation is adopted, the resulting flux of the hyperbolic particles in Fig. 7 is still a factor smaller than that of the IMF model. Furthermore, the gap in number density between the hyperbolic and the main particles becomes larger closer to the Sun, because of their different radial dependencies. As a result, the hump in the number density distribution for particles with masses 10^{-12}g $\leq m \leq 10^{-7}$g becomes larger closer to the Sun.

In case (C)-a, dust input is assumed to increase with a radial dependence of $r^{-3.5}$ until 0.5AU, and to remain constant within 0.5AU. In spite of the radial increase in dust production between 0.5AU and 1AU, the number density distribution for $m \geq 10^{-5}$ is almost constant in case (C)-a. As briefly discussed in the previous section, a slope with $m^{-\frac{7}{3}}$ dependence appears when collisional loss and dust production balance each other out, and the number density in this mass range depends on the radial dependence of the dust input. This means that the number density distribution in this mass range remains constant if the dust input has the same radial dependence. On the other hand, an increase in collisional gain raises the number density for smaller particles. Hence, the line with $m^{-\frac{7}{3}}$ dependence is extended to the less massive particles as the heliocentric distance decreases.

In case (C)-a, inside 0.5AU the radial dependence of dust input is chosen to be constant. Because of this change at 0.5AU, the collisional balance for particles with masses $m \geq 10^{-6}$g is changed, and the number density decreases while keeping a $m^{-\frac{7}{3}}$ dependence. However, the smaller particles that form a $m^{-\frac{4}{3}}$ dependence increase in number because of the dust supply and collisional gain, as well as by geometrical concentration by

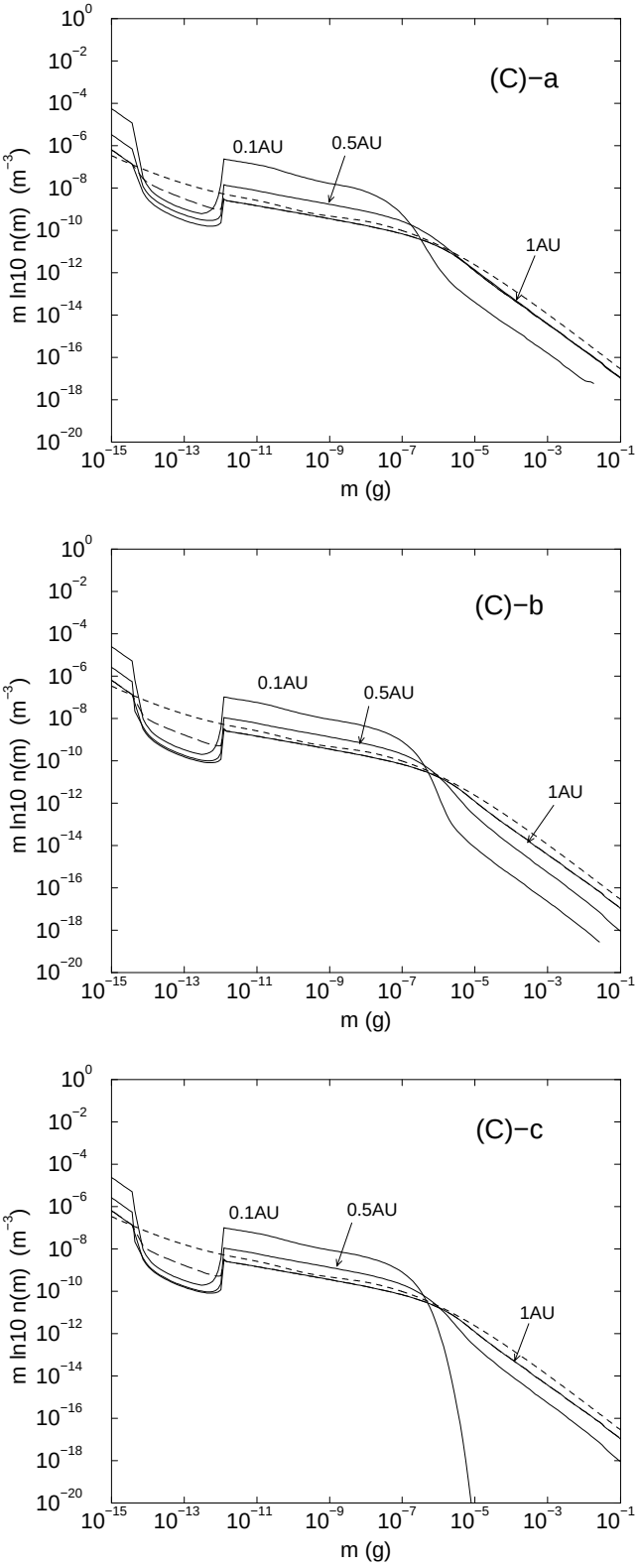

Fig. 7a–c. The calculated number density distribution for case (C)-**a** (upper panel), case (C)-**b** (middle panel), and case (C)-**c** (lower panel). Most of the particles with masses 10^{-14}g $\leq m \leq 10^{-12}$g are of collisional origin and are in hyperbolic orbits. The dashed-line denotes the IMF model at 1AU. The long-dashed line between 10^{-14}g and 10^{-12}g is derived by using the same treatment as in Grün et al. (1985) for particles in hyperbolic orbits at 1 AU.

Poynting-Robertson effects. As a result, around a particle mass of 10^{-6}g, a curve with a new slope in the number density distribution appears to connect the two regions. Once this situation occurs, the number density of the $m \geq 10^{-6}$g particles inside 1AU cannot remain constant with decreasing solar distance, even if the radial dependence of the dust input is the same. Its value decreases as the solar distance decreases due to an excess of $m \leq 10^{-7}$g particles (see case (C)-b). Furthermore, if the dust supply stops at an arbitrary solar distance (case (C)-c), the collisional balance of the large particles can no longer be maintained, and a steep decrease in the number density of large particles occurs, like that seen at 1AU in case (A). In order to form the same trend in the number density distribution as that at 1AU, a steeper increase in dust input has to be added.

4.2. Comparison with observations inside 1AU

Previous estimates of the flux distribution inside 1AU by Grün et al. (1985), which used a biased IMF model, estimated a $r^{-3.5}$ radial dependence for dust sources inside 1AU from the observed radial dependence of $r^{-1.3}$ in the particle number density. (Note that this $r^{-1.3}$ radial dependence is derived from observations of medium-sized particles within 1AU). The numerical results presented here also indicate that a $r^{-3.5}$ dependence in the dust input is required to simulate the mass dependence of the interplanetary dust flux at 1AU. However, a critical point to note in the estimations by Grün et al. (1985) (and also those by Leinert et al. 1983) is that a proportional increase in the number density distribution is assumed for dust particles inside 1AU. As mentioned above, if dust input continues inside 1AU with a $r^{-3.5}$ dependence, the number density of the main particles increases for medium and small particles only (10^{-12}g $\leq m \leq 10^{-7}$g and $m \leq 10^{-14}$g), and the radial increase in medium-sized particles becomes steeper than that expected from a proportional increase in the entire distribution. Hence, the $r^{-1.3}$ dependence in medium-sized particles cannot be explained if the $r^{-3.5}$ radial dependence in dust input is adopted as entirely inside 1AU. Therefore, the radial dependence of the dust supply inside 1AU should be changed elsewhere, as in the three cases assumed in this work.

The upper panel in Fig. 8 shows the resultant number densities for particles with masses 10^{-9}g $\sim 10^{-7}$g ($5\,\mu$m $\sim 20\,\mu$m) for the three dust input scenarios within 1AU, as a function of the heliocentric distance. The lower panel in Fig. 8 is the same as the upper panel, but shows plots of geometrical cross section. The resultant number density and geometrical cross section do not show a proportional increase in the log-scale. As shown in Fig. 8, there are no large differences in the number density and geometrical cross section between cases (C)-b and (C)-c for particles in this mass range. On the other hand, between 0.1AU and 1AU, the values in case (C)-a are significantly larger than those in cases (C)-b and (C)-c. Moreover, in case (C)-a, the radial dependence inside 0.1AU becomes flatter than those in cases (C)-b and (C)-c as the solar distance decreases. This indicates that many particles in the range 10^{-9}g $\sim 10^{-7}$g are destroyed inside 0.1AU due to the increase in the total number

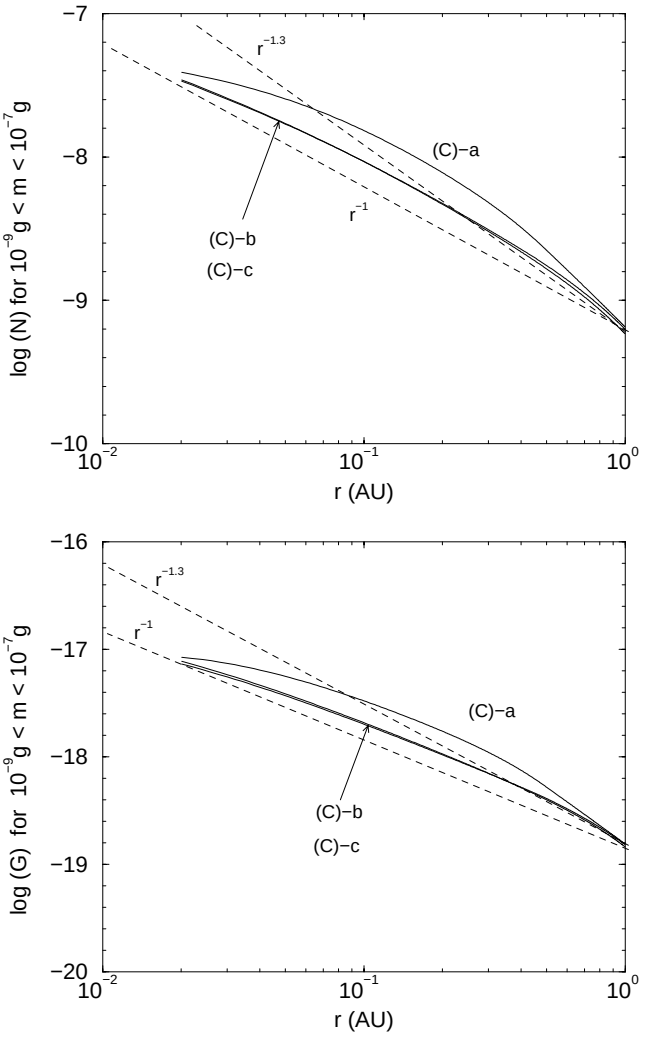

Fig. 8. The number densities (upper panel) and the geometrical cross sections (lower panel) of particles with masses 10^{-9}g $\leq m \leq 10^{-7}$g for cases (C)-a, (C)-b, and (C)-c, as a function of heliocentric distance (solid lines). The dotted lines denote the radial dependencies assumed from the observations of interplanetary dust within 1AU.

density of the particles. In other words, the critical mass m_c in Eq. (25) becomes less than 10^{-7}g. In such a situation, the color ratio of the zodiacal cloud would change significantly with solar distance, even if the mean number density and the geometrical cross section showed a $r^{-1.3}$ dependence. However, significant "bluing" of the zodiacal light with decreasing solar elongation has not been observed.

From these discussions, it seems that cases (C)-b and (C)-c explain the observed interplanetary dust cloud inside 1AU better than case (C)-a. Furthermore, in cases (C)-b and (C)-c, the radial dependencies of the number density and geometrical cross section approach $\sim r^{-1}$ near the Sun ($r \leq 0.1$AU). These agree with the derived radial dependence of $\sim r^{-1}$ from scattering analyses of the solar F-corona (e.g. Mann & MacQueen, 1993). Since the number density distribution inside 1AU does not show the same distribution as that at 1AU, both the observed $r^{-1.3}$ and $r^{-1.0}$ dependencies cannot be demonstrated for interplanetary

dust throughout the vicinity inside 1AU. However, in different radial ranges, the numerical results indicate that both radial dependencies can be explained. Namely, the radial distribution of the interplanetary dust looks like $r^{-1.3}$ between 0.1 and 1AU, and r^{-1} inside 0.1AU.

As shown in Fig. 7, the differences in the resultant number density distributions between cases (C)-b and (C)-c appear only in the mass range $m \geq 10^{-6}$g, and there are no conditions to effectively exclude one of these two models. For a typical model of dust input between 1AU and 5AU, case (C)-b, which includes source (A), is adopted, and is discussed in the following sections by examining its numerical results. Note that the results and discussions in the following sections are almost the same if we adopt model (C)-c instead of model (C)-b.

5. Origin of β-meteoroids

The numerically determined total flux of hyperbolic particles at 1AU is $\sim 1.8 \times 10^{-4}\mathrm{m}^{-2}\ \mathrm{sec}^{-1}$. This is quite consistent with the derived flux of β-meteoroids ($1.5 \pm 0.3 \cdot 10^{-4}\mathrm{m}^{-2}\ \mathrm{sec}^{-1}$) from Ulysses' impact data (Wehry & Mann, 1999). However, the number density distribution of $10^{-14}\mathrm{g} \leq m \leq 10^{-12}\mathrm{g}$ particles at 1AU is about one order of magnitude smaller than that given by the IMF model (see the long dashed line of Fig. 7). As denoted in the previous sections, the derived number density of hyperbolic particles applies only to particles originating from collisions between particles. It corresponds to that of β-meteoroids assumed by Zook (1975) and Zook & Berg (1975).

To increase the flux of hyperbolic particles in our model calculations, a significant dust input inside 1AU is necessary. As a result, the number density of the dust clouds within 1AU increases, and the value becomes unacceptable from the point of view of radial dependence in the total number density. Therefore, in order to explain a flux of hyperbolic particles at 1AU higher than that shown in Fig. 7, some modification of the basic methods adopted in the numerical calculations, or another scenario for the origin of hyperbolic particles, is required.

One meaningful possibility is that the process of fragmentation may differ from the simple power law distribution used here. For example, the Grady-Kipp model of fragmentation (Grady & Kipp, 1980) can produce sub-micron fragments effectively, and the resultant flux of hyperbolic particles will be higher than that shown in Fig. 7 (e.g. Ishimoto, 1997).

Two typical models have been reported for the origin of particles in hyperbolic orbits that do not require a collisional origin. The first possibility is the generation, near the dust free zone, of small particles from large particles by sublimation (e.g. Mukai & Yamamoto, 1979). A point to note is that in this scenario the β ratio of the particles should be greater than unity for them to be in hyperbolic orbits, due to continuous dilution of orbital energy by the effects of sublimation and Poynting-Robertson drag. Under the assumption of "astronomical silicate", the maximum β_{PR} is 0.93 for a 10^{-14}g spherical particle. Although the particles' irregularities may raise their maximum β_{PR} above unity (e.g. Gustafson, 1994), it is not well known whether particles can retain irregularities in the sublimation process. On the other hand, if the zodiacal dust includes a significant portion of carbon-like material, many hyperbolic particles will be generated near the Sun. Therefore, until we know the shape and chemical composition of hyperbolic particles, this scenario is still possible.

A second possibility is that the flux of particles in hyperbolic orbits is not in a steady state, but rather originates from discrete meteor showers by P/Encke-type short-period comets with perihelion distances larger than 0.5AU (Whipple, 1976). Although such discrete events are possible, for them to occur frequently at 1AU would require many unknown comets.

Also of interest is that most of the particles in the $10^{-14}\mathrm{g} \leq m \leq 10^{-12}\mathrm{g}$ mass range at 1AU may be in bound orbits. Indeed, the numerical results calculated under this assumption show good fits to the IMF curve at 1AU, if a specific dust production rate is adopted. However, the resultant number density distribution inside 1AU differs significantly from those in Fig. 7. Since the mean radial velocities of particles in bound orbits are much lower than those of particles in hyperbolic orbits, collisional evolution in the dust cloud as a whole is accelerated by the existence of particles in bound orbits in this mass range, and medium-sized particles then cannot exist inside 0.1AU by collisional destruction, even if dust input inside 1AU is omitted. The existence of particles in hyperbolic orbits acts to restrain the acceleration of collisional evolution in the zodiacal cloud. For these reasons, it can be said that a significant proportion of particles is required to be in hyperbolic orbits to sustain the dust environment observed within 1AU. The same conclusion has been made in a previous work (Ishimoto, 2000).

Since a reliable value for the dust flux in the aforementioned mass range has not yet been confirmed, no conclusions can be drawn as to the origin of particles in hyperbolic orbits (or β-meteoroids) from the numerical results of collisional evolution.

6. Effects of hyperbolic and interstellar particles beyond 3AU

Since the discovery of the influx of interstellar particles from dust measurements by Galileo and Ulysses (e.g., Grün et al., 1993, 1995a, 1995b), they have been assumed to be an important component of the dust population in the outer solar system. Moreover, further analyses have indicated that interstellar particles exist, at least, beyond 3AU near the ecliptic plane, and beyond 1.8AU at high ecliptic latitudes (e.g. Grün et al., 1997).

In the final step of the model calculations, interstellar influx is included. Although a mean mass of 3×10^{-13}g, a mean flux of $1.5 \times 10^{-4}\mathrm{m}^{-2}\ \mathrm{sec}^{-1}$, and a mean influx velocity of ~ 26 km sec^{-1} (Grün et al., 1997) have already been reported, some of the physical parameters of the interstellar dust population, such as the radial dependencies of the flux and particle size distribution, are not accurately known. Therefore, as a test, a log-normal distribution consistent with the above known parameters is adopted for the mass distribution of the interstellar dust flux at 5AU. This is adopted only to avoid the gaps generated in the number density distribution of the main particles. Also, a simple radial dependence for the interstellar flux $f_{is}(r)$

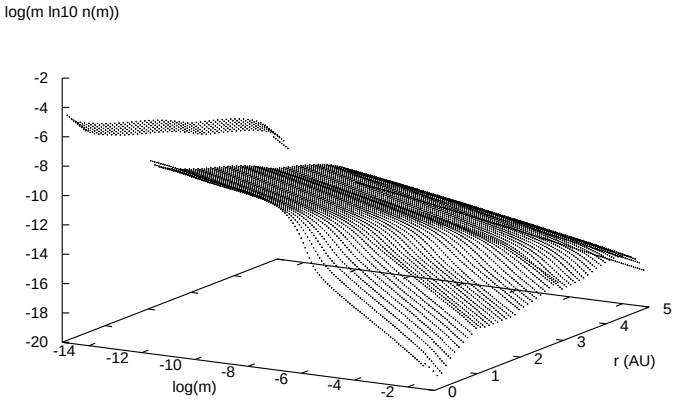

Fig. 9. An overview of the number density distribution within 5AU calculated from simulations of the collisional evolution of particles, without interactions by hyperbolic and interstellar particles. Model (C)-b has been adopted for the dust source.

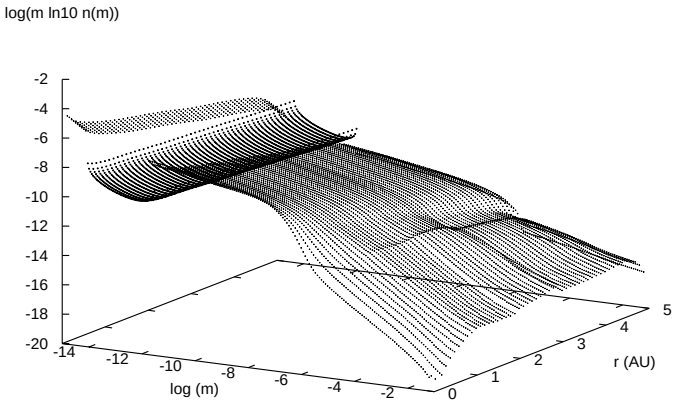

Fig. 10. Same as Fig. 9 but taking collisional interactions by hyperbolic particles into account.

is assumed.

$$f_{is}(r) = \frac{r-3}{2} f_{is}(5\mathrm{AU}) \qquad (3 \le r \le 5\mathrm{AU})$$
$$= 0 \qquad (0 \le r < 3\mathrm{AU}). \tag{32}$$

Figs. 9-11 are the calculated number density distributions when the following are considered, respectively: the main particles, the main and generated hyperbolic particles, and the main, hyperbolic, and interstellar particles. Fig. 12 shows the radial dependence of the number density of medium-sized particles for the cases shown in Figs. 9-11. From Figs. 9-11 and Fig. 12, we found that collisions by hyperbolic and interstellar particles drastically increase the number density of interplanetary dust particles with masses $m \le 10^{-7}$g beyond 3AU. From Eqs. (16) and the model of interstellar particles, the main particles, vulnerable to collisions with hyperbolic and interstellar particles, have an upper mass of about $m \sim 10^{-6}$g. As the $m \sim 10^{-6}$g particles are destroyed, their fragments increase the number density of the $m \le 10^{-6}$g particles. An excess of $m \le 10^{-6}$g particles in the collisional balance then acts to destroy the $m \sim 10^{-3}$g particles, and the number density of the $m \le 10^{-3}$g particles is increased by the fragments of the $m \sim 10^{-3}$g particles. In such

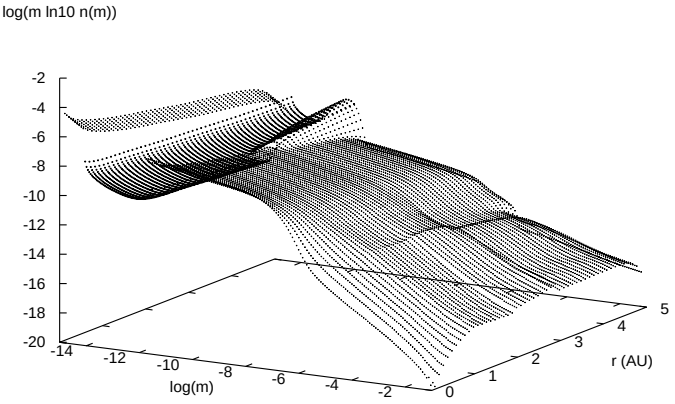

Fig. 11. Same as Fig. 9 but with the collisional interactions by hyperbolic and interstellar particles taken into account. The number density distribution of the interstellar particles and its radial dependence is described in the text.

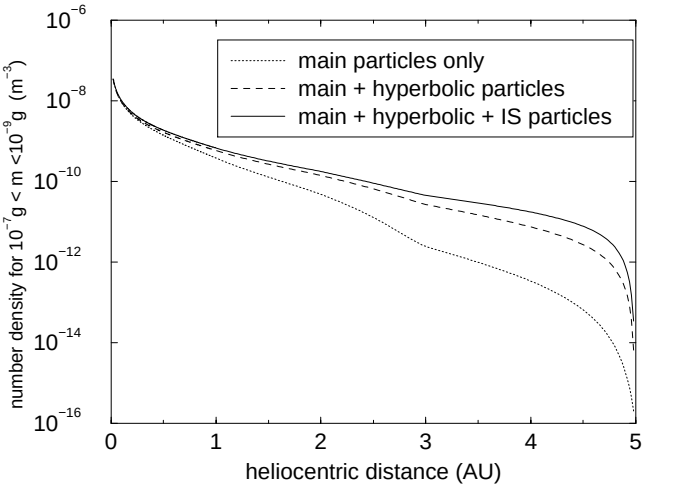

Fig. 12. The number densities for the medium-sized particles ($10^{-9}\mathrm{g} \le m \le 10^{-7}\mathrm{g}$) in the cases shown in Figs. 9-11 as a function of heliocentric distance.

a collisional cascade, the number density of the $m \le 10^{-7}$g particles increases continuously. However, due to radial velocities imparted by the Poynting-Robertson and solar wind drag forces on the $m \le 10^{-7}$g particles, the feedback of this collisional cascade is imperfect, and the increase in number density stops when a new collisional balance, shown in Figs. 10 and 11, is established. From these results, the number density of medium-sized (from a micron to several tens of microns) interplanetary dust is expected to maintain a relatively flat radial distribution, even beyond the asteroid belt, if the above model of interstellar flux is realistic. Since the flux of hyperbolic particles decreases significantly outside 5AU, the above collisional cascade by hyperbolic particles is not effective outside 5AU. On the other hand, interstellar particles could cause such a collisional cascade, even outside 5AU, if some impact targets exist that can produce dust particles by collision with the interstellar particles. According to Pioneer observations (Humes, 1980), the flux of interplanetary particles with masses $m \ge 10^{-10}$g shows a flat radial dependence. Furthermore, the existence of

micron-sized particles between 6 and 51AU has been reported by authors who analyzed the records of Voyager's plasma wave instruments (Gurnett et al., 1997). Although it is possible to explain these data by the interstellar particles themselves, by the particles ejected from collisions between EKOs (e.g. Liou et al., 1996), or by cometary ejecta (Gurnett et al., 1997), the data can also be explained by fragments induced by, for example, impacts of interstellar particles with comets or large cometary particles at aphelion distances.

Although hyperbolic particles as well as interstellar particles within 5AU cause the collisional cascade denoted above, the number density of medium-sized particles in the case without interstellar particles is smaller than that in the case which considers interstellar particles outside 3AU. Inside 5AU, further knowledge of the flux of interstellar particles is required to construct a realistic model for the number density distribution of interplanetary dust. According to the observations by Galileo and Ulysses, the flux of interplanetary dust decreases significantly beyond 3AU (e.g. Grün et al., 1997). This indicates that the collisional cascade may not work as effectively as that shown in Fig. 11, and the number density distribution of the interplanetary dust may be rather similar to that shown in Fig. 10.

7. Cometary or asteroidal?

As already mentioned in Sect. 3, dust sources with a radial dependence of $r^{-3\sim4}$ that supply large dust particles directly at 1AU are required to simulate the flux curve of the interplanetary dust at 1AU, for particles with masses $m \geq 10^{-6}$g. Furthermore, the possibility of short period comets being the origin of such dust has been discussed. However, in our opinion, the importance of asteroidal particles should not be discounted. Many authors have proposed that asteroidal particles are an important component of the zodiacal cloud, both for asteroidal dust bands and for the Earth's resonant rings (e.g., Dermott et al., 1994, Jayaraman & Dermott, 1996, Grogan et al., 1997, Durda & Dermott, 1997, Reach et al., 1997, Kortenkamp & Dermott, 1998). Between 1AU and 3AU from the Sun, asteroidal particles are probably the dominant component of zodiacal clouds, at least for particles with masses $10^{-12}\text{g} \leq m \leq 10^{-6}$g. However, are they also the major component within 1AU? The results of our numerical estimation indicate that the major population of zodiacal clouds may be changed elsewhere in the solar system due to collisional evolution. Since, at 1AU, cometary particles are numerically of the same order of magnitude as asteroidal particles with masses $m \leq 10^{-7}$g, it can be expected that the major component may change in the course of particles' collisional evolution, because of cometary dust supply and also because of the destruction of particles with masses $m \geq 10^{-6}$g within 1AU. Furthermore, the transition will occur relatively near 1AU, but not deep inside 1AU. According to observations by the IRAS spacecraft and the ZIP rocket, within 1AU of the Sun the local albedo of the zodiacal cloud increases as the solar distance decreases (e.g. Levasseur-Regourd et al., 1991). Although some physical processes, such as a change in the particles' porosity, roughness, darkness and size with solar distance (e.g. Levasseur-Regourd et al., 1990, Mukai et al., 1986) are possible explanations for the increase in the local albedo, a radial change in the mixing rate between asteroidal and cometary particles might cause the same effect in the bulk feature of the zodiacal cloud.

8. Dust avalanche

In the numerical methods of this paper, the equilibrium state of dust clouds is examined under the assumption of a constant dust input from the parent bodies. However, it is not clear whether the zodiacal cloud is in a state of equilibrium at the present time. Furthermore, the iterative calculations denoted in Sect. 2 do not converge in the case of an enormous input of dust.

Although hyperbolic particles act to restrain collisional evolution in the zodiacal cloud at the present time, they might seriously affect the evolution of the dust cloud if their number density exceeded a critical value. If the small particles generated in hyperbolic orbits can destroy all the particles in circular orbits at solar distance r, then dust particles cannot enter inside r. Furthermore, the production of an enormous number of hyperbolic particles might act to clean up the dust environment throughout the planetary system. Such a "dust avalanche" has been predicted in the dust environment of β-Pictoris (Artymowicz, 1997). Here, a quantitative estimation for a dust avalanche is made for our solar system of interest, to provide an overview of the collisional evolution of dust clouds.

Assuming that particles with mass m', number density distribution $n(m', r)$, on circular orbits at solar distance r, disappear at distance r_a ($r_a < r$) due to collisional destruction by hyperbolic particles, the derivative $\partial n(m', r)/\partial r$ in Eq. (1) can be written approximately as

$$\frac{\partial n(m', r)}{\partial r} \sim \frac{n(m', r)}{r - r_a}. \tag{33}$$

For simplicity, we neglect the dust production terms in Eq. (2). Substituting Eq. (14) into Eq. (1)

$$\begin{aligned} \frac{2r - r_a}{r(r - r_a)} \;=\; & -\frac{1}{v_r(m', r)} \int_{m_{h0}}^{m_{h1}} n(m_h, r) \\ & \cdot\sigma(m', m_h)\, v_i(m_h, r)\, dm_h, \end{aligned} \tag{34}$$

where m_{h0} and m_{h1} are the minimum and maximum masses of the hyperbolic particles respectively. The number density distribution of the generated hyperbolic particles $n(m_h, r)$ is

$$n(m_h, r) = \int_{r_a}^{r} \frac{1}{v_r(m_h, r')} \left(\frac{r'}{r}\right)^2 \frac{dn_g(m_h, r')}{dt} dr'. \tag{35}$$

If we know the mass dependence of $n(m, r)$ for the particles in circular orbits between r and r_c, we can derive $n(m, r)$ by substituting Eq. (13) and Eq. (35) into Eq. (34).

For a simple estimation, a mass dependence of $m^{-\frac{4}{3}}$ and a radial dependence the same as that in Eq. (33) are adopted in

Eq. (13). After making some approximations, $n(m', r)$ is derived as

$$n(m', r) \sim 2.9 \, \frac{\rho^{\frac{2}{3}} G^{\frac{1}{4}} M_{\odot}^{\frac{1}{4}}}{r^{\frac{3}{4}}} \sqrt{\frac{\beta(m') \, (2r - r_a)}{c(r - r_a) D_1 D_2 D_3}} \; m'^{-\frac{4}{3}} \quad (36)$$

where,

$$D_1 = \int_{m_0}^{m_1} m_p^{-\frac{4}{3}} dm_p \int_{m_0}^{m_1} m_t^{-\frac{2}{3}} \left(m_t^{\frac{1}{3}} + m_p^{\frac{1}{3}} \right)^2 dm_t$$

$$D_2 = \int_{m_{h0}}^{m_{h1}} m_h^{-\frac{5}{3}} \left(m'^{\frac{1}{3}} + m_h^{\frac{1}{3}} \right)^2 dm_h$$

$$D_3 = \int_{r_a}^{r} \left(\frac{r'}{r} \right)^{\frac{3}{2}} \left(\frac{r' - r_a}{r - r_a} \right)^2 dr'$$

m_0 and m_1 are, respectively, the minimum and maximum masses of the particles in circular orbits that can be destroyed by collisions with hyperbolic particles. If $(r - r_a) = \delta r \ll r$, Eq. (36) can be rewritten as

$$n(m', r) \sim 5.0 \, \frac{\rho^{\frac{2}{3}}}{\delta r} \left(\frac{G M_{\odot}}{r} \right)^{\frac{1}{4}} \sqrt{\frac{\beta(m')}{c D_1 D_2}} \; m'^{-\frac{4}{3}}. \quad (37)$$

The distribution $n(m'r)$ for $r = 1$AU and $\delta r = 0.01$AU is shown by the dashed line in Fig. 13. The mass m_0 is 10^{-12}g, and the two dashed lines correspond to different values of m_1 (10^{-7}g and 10^{-9}g). If the number density distribution at 1AU for particles with mass $m = 10^{-7}$g exceeds that of the lower dashed line in Fig. 13, the particles generated in hyperbolic orbits can destroy most of the 10^{-7}g particles between 1AU and 0.99AU. It can be deduced from the above equations that the mass dependence of the dashed lines is about $m^{-\frac{11}{6}}$. Therefore, some particles between 1AU and 0.99AU with masses less than 10^{-7}g can survive the destruction by the hyperbolic particles generated. However, the destruction of the 10^{-7}g particles produces many particles with masses less than 10^{-7}g. Thus the number density curve of the particles with masses less than 10^{-9}g easily exceeds the upper dashed line in Fig. 13 between 0.99AU and 1AU. In this way, the number density distribution of particles increases along the solid line in Fig. 13. The solid line in Fig. 13 is calculated using the above equations, but with m' substituted into m_1 for D_1. From these estimations, it can be said that the solid line in Fig. 13 is a kind of forbidden line, and a dust avalanche will occur if the number density curve of the interplanetary particles touches this forbidden line.

As seen in Eq. (37), the level of the forbidden line is proportional to $1/\delta r$. Roughly speaking, the level of the forbidden line in Fig. 13 decreases by two orders of magnitude if δr is set to 1AU ($r_a \to 0$). This indicates that a dust avalanche will occur within 1AU if the number density of the interplanetary dust for 10^{-7}g particles is three orders of magnitude higher than that at the present time at 1AU. The most massive particles that can be destroyed catastrophically by the hyperbolic particles weigh about 10^{-7}g. Therefore, the forbidden line defined above cannot be extended to particles with masses $m > 10^{-7}$g. If we consider erosive impacts by hyperbolic particles, however, the extended line (long-dashed line in Fig. 13) is also expected to show the indirect critical values for triggering a dust avalanche.

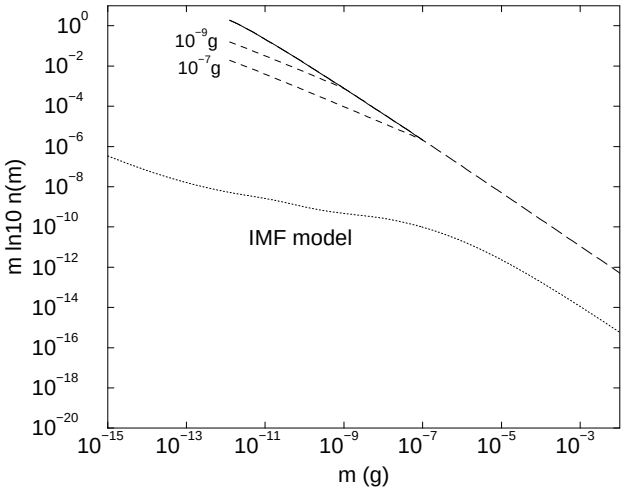

Fig. 13. The critical values in the number density distribution for the occurrence of a "dust avalanche" between 0.99AU and 1AU. The lower and upper dashed lines are the results of Eq. (37) for target particles with maximum masses of 10^{-7}g and 10^{-9}g respectively. The solid line is the assumed "forbidden line" for the number density of dust particles (see text). The dotted line corresponds to the IMF model at 1AU.

It is hard to assume that a dust avalanche occurs in a stationary state. However, a discrete dust production event, for example just after the collisional destruction of a large asteroid or comet, might cause the same effects, even in the solar system.

9. Conclusions

Using some model calculations for the equilibrium number density equations, the relationship between dust input and the appearance of the number density distribution was examined, taking the collisional process into account as well as dynamic evolution influenced by the Poynting-Robertson effect, and an approach to estimate the parent bodies of interplanetary dust from the observed number density distribution was discussed.

The number density distribution of interplanetary dust at 1AU suggests that collisional gain and loss are balanced out for particles with masses $m \geq 10^{-6}$g, while particles in the mass range $10^{-12}\text{g} \leq m \leq 10^{-7}$g show a mass dependence described by collisional gain and Poynting-Robertson orbital decay. To simulate this number density distribution at 1AU, a considerable amount of direct dust input at 1AU is necessary. Furthermore, the numerical result for the number density distribution in the case where the dust input has a radial dependence of $r^{-3\sim-4}$ outside 1AU shows good agreement with that of the Interplanetary Meteoroid Flux model. Such a dust source would be comets rather than asteroids, and this indicates that the contribution of cometary dust at 1AU is important, in addition to the assumed contribution of asteroidal dust. Furthermore, the importance of cometary dust increases as the heliocentric distance decreases, because of the collisional destruction of large cometary particles.

Applying a $r^{-1\sim-1.3}$ radial dependence in the observed number densities of the interplanetary dust inside 1AU, it is estimated that the dust input that has a radial dependence of $r^{-3\sim-4}$ outside 1AU will be either constant or decreasing as the solar distance decreases within 1AU. The resultant flux of particles in hyperbolic orbits by particle collisions is $\sim 1.8\times10^{-4}\mathrm{m}^{-2}$ sec^{-1} at 1AU. Although this is consistent with the flux of β-meteoroids derived from Ulysses' impact data, it is a factor smaller than that predicted by the IMF model.

Using these results for the estimated dust input by parent bodies, the number density distribution within 5AU of the Sun was examined. Collisional interactions between bound particles and interstellar/hyperbolic particles cause an imperfect collisional cascade, and increase the number density of medium mass particles. Conclusively, the number density of particles with $10^{-12} \leq m \leq 10^{-7}$g will not decrease drastically within 5AU, even far from the asteroid belt. Moreover, this collisional interaction may play an important role in determining the interplanetary dust environment outside 5AU, if the influx of interstellar particles is effective.

As discussed in the text, the number density distribution of dust particles strongly depends on the dust production rate of the parent bodies and its radial dependence. Therefore, it is not realistic to apply the trend seen in the number density distribution of the dust particles in the IMF model to an arbitrary solar distance. Furthermore, collisional interactions in the outer solar system, such as those by interstellar particles, could easily change the general trend in the number density distribution in a region.

Particles in hyperbolic orbits in our solar system act to restrain the acceleration of collisional evolution in the zodiacal cloud inside 1AU. However, in another planetary system, e.g. β-Pic., the role of hyperbolic particles may differ from that in our solar system. In particular, the "dust avalanche" process proposed by Artymowicz (1997) may occur under some planetary conditions. Even for our solar system, some discrete events might change the total dust environment drastically. Possibilities include collisions of large asteroids, or an elevation of the flux of interstellar particles by several orders of magnitude. However, some improvements to the numerical approaches used in this paper are needed to model the dust environment for such discrete events exactly.

Although the numerical approaches described in this paper are adopted mainly to search for an acceptable dust source distribution that explains both dust flux at 1AU and some of the observed properties of interplanetary dust, the basic advantage of these approaches is that they can estimate directly the number density distribution of dust particles at an arbitrary solar distance by taking collisional processes into account, even without information on the dust particles at that location. Furthermore, it is easy to change some of the initial conditions, such as the luminosity of the central star, the material of the impact ejecta, the mass production rate, and the radial dependence of the dust sources. By modifying these initial conditions, it is possible to study past and future dust environments of the solar system, as well as those of other planetary systems.

Acknowledgements. The author wishes to thank Dr. M. K. Landgraf for some important comments. The review by Dr. V. Dikarev and Prof. E. Grün has contributed greatly to the publication of this paper.

References

Artymowicz P., 1997, Annu. Rev. Earth Planet. Sci. 25, 175
Banaszkiewicz M., Ip H., 1991, Icarus 90, 237
Burns J.A., Lamy P.L., Soter S., 1979, Icarus 40, 1
Dermott S.F., Jayaraman S., Xu Y.L., Gustafson B.Å.S., Liou J.C., 1994, Nat 369, 719
Draine B.T., Lee H.M., 1984, AJ 285, 89
Durda D., Dermott S.F., 1997, Icarus 130, 140
Flynn G.J., 1994, Proc. 25th Lunar Planet. Sci. Conf., 379
Grady D.E., Kipp M.E., 1980, 1st J. Rock Mech. Min. Sci. & Geomech. Abstr. 17, 147
Grogan K., Dermott S.F., Jayaraman S., Xu Y.L., 1997, Planet. Space Sci. 45, 12; 1657
Grün E., Zook H.A., Fechtig H., Giese R.H., 1985, Icarus 62, 244
Grün E., Zook H.A., Baguhl M., et al., 1993, Nat 362, 428
Grün E., Baguhl M., Divine N., et al., 1995a, Planet. Space Sci. 43, 953
Grün E., Baguhl M., Divine N., et al., 1995b, Planet. Space Sci. 43, 971
Grün E., Staubach P., Baguhl M., et al., 1997, Icarus 129, 270
Gurnett D.A., Ansher J.A., Kurth W.S., Granroth L.J., 1997, Geophys. Res. Lett. 24, 3125
Gustafson B.Å.S., 1994, Annu. Rev. Earth Planet. Sci. 22, 553
Humes D.H., 1980, J. Geophys. Res. 85, 5841
Ishimoto H., 1997, Adv. Space Res. 20, 1523
Ishimoto H., 1998, Earth Planets Space 50, 521
Ishimoto H., Mann I., 1999, Planet. Space Sci. 47, 225
Ishimoto H., 2000, Adv. Space Res. 25, 281
Jayaraman S., Dermott S.F., 1996, In: Gustafson B.Å.S., Hanner M.S. (eds.) Physics, Chemistry, and Dynamics of Interplanetary Dust. Brigham Young Univ., Provo, p. 155
Keller H.U., 1990, In: Huebner W.F. (ed.) Physics and Chemistry of Comets. Springer-Verlag, Berlin/New York/Tokyo, p. 13
Kessler D.J., 1981, Icarus 48, 39
Kimura H., Mann I., Mukai T., 1998, Planet. Space Sci. 46, 911
Kortenkamp S.J., Dermott S.F., 1998, Icarus 135, 469
Lamy P.L., 1974, A&A 35, 197
Levasseur-Regourd A.C., Dumont R., Renard J.B., 1990, Icarus 86, 264
Levasseur-Regourd A.C., Renard J.B., Dumont R., 1991, In: Levasseur-Regourd A.C., Hasegawa H. (eds.) Origin and evolution of interplanetary dust. Kluwer, Japan, p. 131
Leinert C., Richter I., Pitz E., Planck B., 1981, A&A 103, 177
Leinert C., Röser S., Buitrago J., 1983, A&A 118, 345
Liou J.C., Dermott S.F., Xu Y.L., 1995, Planet. Space Sci. 43, 717
Liou J.C., Zook H.A., Dermott S.F., 1996, Icarus 124, 429
Mann I., MacQueen R.M., 1993, A&A 275, 293
Mazets E.P., Aptekar R.L., Golenetskii S.V., et al., 1986, Nat 321, 276
McDonnell J.A.M., Gardner D.J., McBride N., 1996, In: Gustafson B.Å.S., Hanner M.S. (eds.) Physics, Chemistry, and Dynamics of Interplanetary Dust. Brigham Young Univ., Provo, p. 193
McDonnell J.A.M., 1978, In: McDonnell J.A.M. (ed.) Cosmic Dust. Wiley, Chichester, p. 337
Mukai T., Yamamoto T., 1979, PASJ 31, 585
Mukai T., Fechtig H., Grün E., Giese R.H., Mukai S., 1986, A&A 167, 364

Mukai T., 1989, In: McNally D. (ed.) Highlights of Astronomy 8, p. 305
Nakamura A., Fujiwara A., 1991, Icarus 92, 132
Reach W.T., Franz B.A., Weiland J.L., 1997, Icarus 127, 461
Sykes M.V., Walker R.G., 1992, Icarus 95, 180
Tielens A.G.G.M., McKee C.F., Seab C.G., Hollenbach D.J., 1994, ApJ 431, 321
Wehry A., Mann I., 1999, A&A 341, 296
Whipple F.L., 1976, In: Elsässer H., Fechtig H. (eds.) Interplanetary Dust and Zodiacal Light. Springer-Verlag, New York, p. 403
Wyatt S.P., Whipple F.L., 1950, ApJ 111, 134
Zook H.A., 1975, Planet. Space Sci. 23, 1391
Zook H.A., Berg O.E., 1975, Planet. Space Sci. 23, 183